Recent developments in ICRF antenna modelling

P.U. Lamalle, A.M. Messiaen, P. Dumortier and F. Louche

Laboratory for Plasma Physics, Association EURATOM - Belgian State, partner in the Trilateral Euregio Cluster, Royal Military Academy, 30 av. de la Renaissance, B-1000 Brussels, Belgium.

e-mail contact of main author: Philippe.Lamalle@rma.ac.be

Abstract.
The antennas presently developed for ICRF heating of the ITER plasma consist of a tightly packed array of a large number of radiating straps, in order to deliver a high power density without exceeding radio-frequency voltage standoffs. Recently developed commercial software has enabled important progress in the coupling analysis and optimisation of such demanding systems. Approximations allowing to convincingly include a realistic plasma description in these codes are discussed. Application of the resulting numerical tools is illustrated by simulation of the existing JET A2 ICRF array, with the goal to validate simulations for future antennas. Advances in the design of realistic test bed conditions, using salted water as a means of creating plasma-relevant antenna loading, and the appropriate scaling of a mockup are also presented.

1. Introduction

The antenna systems presently developed for ion cyclotron resonance frequency (ICRF) heating of the ITER plasma [1, 2] consist of an array of a large number of radiating straps, 16 to 24 depending on design options. Such a large number is needed to deliver the high power density (~8MW/m^2) required for the launcher without exceeding the radio-frequency (RF) voltage standoff of its straps. The straps will unavoidably be mutually coupled as they are radiating in the same medium. A proper prediction of the antenna coupling properties is an essential ingredient in estimating the performance of future ICRF antenna systems, such as the ITER and JET ITER-Like [3] ones. This is a notably complex problem, which demands the evaluation of both input resistance and reactance matrices of the antenna array. The reactance matrix requires detailed calculation of near fields and self-consistent surface currents on complex metallic structures. The resistance matrix sensitively depends on the distance between the plasma edge and the antenna and on the detailed plasma density profile, with a high sensitivity to pedestal, scrape-off and far scrape-off parameters. There is considerable uncertainty on the latter parameters for ITER, and its ICRF antenna design calculations must accommodate worst case assumptions. Progress has recently been made in this modelling [4, 5, 6] by application of modern three-dimensional (3D) electromagnetic simulation tools [7, 8], which have become quite powerful and user-friendly since the last generation of antennas were designed. A successful comparison between the simulated reactance matrix of the JET A2 antenna [9] radiating in vacuum and earlier low power measurements on an antenna prototype [10] has recently been carried out [6]. Such simulations in the absence of plasma provide important information on RF surface current and electric field distributions as well as useful code benchmarking. However they do not at all represent the radiation properties of the antenna in presence of plasma. Although the commercial electromagnetic codes [7, 8] include the description of anisotropic dielectrics and of some frequency dispersive media including ferrites, they do not allow the direct modelling of a magnetized plasma, which requires a gyrotropic dielectric permittivity tensor. We have developed a remedy to this limitation, valid within the scope of designing ICRF antennas – i.e. well suited for computing their equivalent input parameters and estimating RF fields and currents on their conductors.

Indeed, we show in Section 2 that a dielectric slab with large dielectric constant facing an ICRF antenna in vacuum can adequately simulate a plasma with steep edge such as occurs in ELMy H Mode, the standard mode of operation foreseen for ITER. The large discontinuity in dielectric constant at the dielectric boundary captures the essential features of wave reflection and refraction in the plasma edge. More refined representations of the edge can be obtained with a multi-layered dielectric. In practice the equivalent dielectric permittivity is determined by comparison of its spectral Green function with that of a plasma in the BRACC coupling code [11], which uses a simple strip line approximation of the antenna straps. The resulting dielectric is implemented in the detailed 3D model of the antenna. This approach is applied in an ongoing three-dimensional study of the JET A2 antenna [6] with the CST MICROWAVE STUDIO® (MWS) software [7], presented in Section 3. The other important practical application of the equivalent dielectric medium, presented in Section 4, is the ability to test the complete antenna system on a mockup, where the plasma loading can be simulated in very simple and cost-effective fashion by a salted water tank [12].

2. Use of dielectric or electrolyte to simulate the plasma loading of ICRH antennas

Antenna modelling used for the comparison plasma-dielectric. The JET-EP and ITER antenna arrays are made of sections of strip lines (or straps) short-circuited to a background plane. The induced e.m.f. method [13, 14, 15] is used to compute the input impedance of the radiating straps in the ANTITER [16] and BRACC [11, 17] codes. It consists of assuming that the antenna current is known and to compute the radiated complex power P from the work done on this antenna current by the induced electric field. The plane geometry model describing a pair of radiating straps is shown in Fig. 1 together with the notations used for their geometry. The straps can be displaced in the the z (toroidal) and y (poloidal) directions and are situated at a distance *d* of the metal wall and at a distance *a* of the plasma or dielectric boundary. Following an $\exp(-i\omega t+ik_z z+ik_y y)$ Fourier analysis, the radiated power P can be expressed by the sum of its $TE|_z$ and $TM|_z$ components, given by the following expressions [13, 14, 15]:

$$2P_{TE}=-(\omega\mu_0/4\pi^2)\iint\Psi dk_z dk_y \; ; \qquad 2P_{TM}=-(\omega\varepsilon_0 4\pi^2)^{-1}\iint X dk_z dk_y \tag{1}$$

The spectral functions $\psi\cong f_1(\xi_1)f_2(J_x,J_y)$ and $X=f_3(\xi_2)f_4(J_x,J_y)$ are functions of the surface current distributions J_y along the straps and J_x along their feeders and of the surface impedances at the plasma or dielectric boundary: $\xi_1=E_y/(\omega B_z)|_{x=-a}$ and $\xi_2=E_z/(\omega B_y)|_{x=-s}$ are respectively the k_y, k_z spectra of the surface impedance for the $TE|_z$ and $TM|_z$ waves. If the periodicity along the y and z directions with respectively periods $2\pi r$ and $2\pi R$ is taken into account the Fourier integrals are replaced by Fourier series for $k_z=m/R$ and $k_y=n/r$ [16]. The antenna straps are considered as lossy strip lines. Their distributed resistance R_A, inductance L_A, conductance G_A and capacitance C_A can be obtained from the energy conservation in a transmission line:

$$2P_{TE} + 2P_{TM} = (R_A-i\omega L_A)\int_0^{2wy}|I(y)|^2dy + (G_A-i\omega C_A)^{-1}\int_0^{2wy}|dI(y)/dy|^2dy \tag{2}$$

It is shown in [16] that R_A and L_A are derived from P_{TE} and G_A and C_A from P_{TM}. In presence of an electrostatic screen in front of the straps only the TE waves are coupled to the plasma (or dielectric) and the TM power is purely reactive ($G_A=0$). The TE wave is excited by the current I(y) flowing along the strap whereas the TM wave by its derivative i.e. by the voltage on the strap. It results that the TM waves are not significantly excited in short-circuited straps of length $2w_y<<\lambda_0=2\pi c/\omega$ even if there is no electrostatic screen. From the knowledge of R_A, L_A, G_A, C_A the input impedance Z_A of the strap is computed by the transmission line relations. In what follows we consider the loading due to the TE wave launched into the plasma or dielectric medium under single pass absorption conditions.

Wave dispersion in a uniform plasma or dielectric. If the medium x<-a is uniform and semi-infinite the wave Fourier components propagate in it with the spatial dependence $\exp(-i\rho x+ik_z z+ik_y y)$. The radial wavenumber ρ has the following expressions (see Fig. 2): *(i)* For the fast magnetosonic wave excited by a TE|$_z$ wave in a magnetised plasma $\rho_p=(k_\perp^2-k_y^2)^{1/2}$ where $k_\perp^2$ is a function of k_z, the plasma density *n*, the steady magnetic field B assumed and the angular frequency $\omega=2\pi f$. For $k_y=0$ the wave will propagate in the domains where $k_\perp^2>0$. A typical locus of propagating waves in the k_z, k_y plane is shown in Fig. 2. This domain shrinks when $k_y\neq 0$. In the figure $\beta_i=\omega_{ci}/\omega$ where ω_{ci} is the ion cyclotron frequency. If $k_z^2=k_0^2$ then $k_\perp=\omega/V_A$ where $V_A=c\omega_{ci}/\omega_{pi}$ is the Alfvén velocity. *(ii)* If the region x<-a is vacuum then $\rho_v=(k_0^2-k_z^2-k_y^2)^{1/2}$ with $k_0=\omega/c$. The corresponding wave propagation domain in the k_z, k_y plane is much smaller. *(iii)* If the region x<-a is filled with a dielectric then $\rho_D=(k_0^2K_D-k_z^2-k_y^2)^{1/2}$ where K_D is its dielectric constant. When K_D is large (which is the case with water) the propagation domain in the k_z, k_y plane also becomes much larger than for vacuum and, for well chosen K_D, can be made similar to the propagation domain of the plasma.

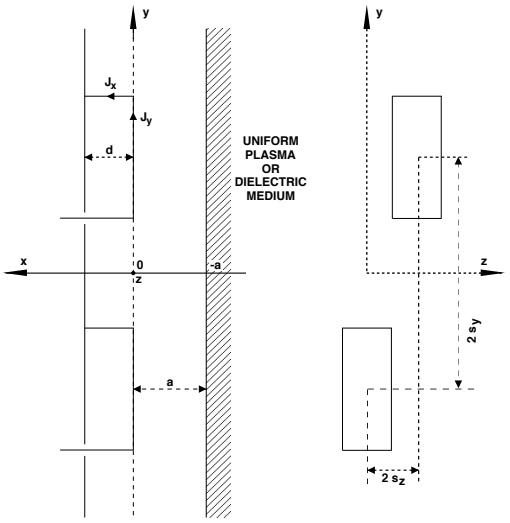

FIG. 1. Layout of the strip line antenna model facing the plasma or dielectric medium.

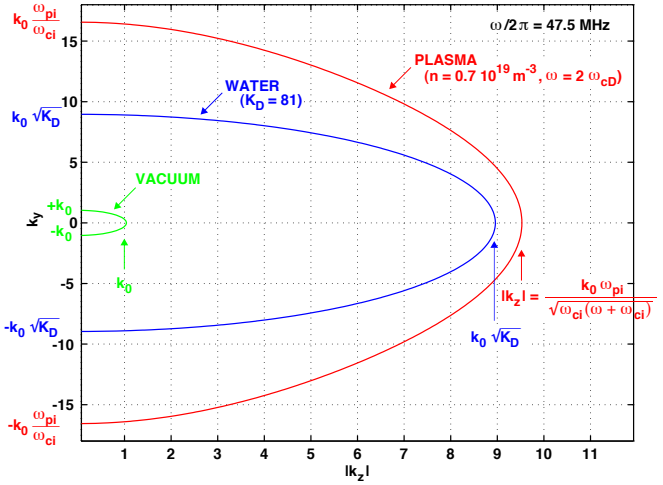

FIG. 2. Wave cutoffs in the $|k_z|$, k_y plane ($\omega/2\pi$=47.5MHz) for (i) the fast magnetosonic wave in a uniform plasma (n=0.7 $10^{19}m^{-3}$, $\omega=2\omega_{cD}$,), (ii) vacuum, (iii) pure water (K_D=81). The domains of propagation are inside the indicated boundaries.

Antenna loading by plasma and dielectric with sharp edge. They are qualitatively similar and can even be made close quantitatively if the value of K_D is well chosen. Indeed, the main effect of the plasma is to provide a jump in the perpendicular propagation constant at x=-a. The same effect is also obtained by replacing the plasma by a large $|K_D|$ medium: the waves inside the dielectric will propagate for $k_z^2+k_y^2<\mathrm{Re}(K_D\,k_0^2)$. The increase of K_D (or the ratio c/V_A for the plasma case) allows to expand the range of k_z and k_y spectrum excited by the current distribution on the straps that can be coupled to the dielectric or plasma half-space. This results in an increase of the antenna loading. The effect of coupling increase by raising K_D is nevertheless counteracted by *(i)* the tunnelling effect of the waves with $k_z^2+k_y^2> k_0^2$ which are more and more attenuated in the space between the straps and the dielectric surface at x=-a when $k_z^2+k_y^2$ increases; *(ii)* the reflection at the jump of perpendicular propagation constant at x=-a. For instance in the case of a plane wave with $k_y=k_z=0$ impinging the transition layer at x=-a, the field reflection coefficient is $(\eta_D-\eta_0)/(\eta_D+\eta_0)$ where η is the intrinsic impedance of the medium. This reflection also allows the excitation of “coaxial

modes" [18] which propagate between the metal wall (at x=d) and the dielectric or the plasma surface, or even of a surface wave [17] along the low density edge of a non uniform plasma.
Fig. 3a shows a typical TE power spectrum for the case of water (K_D=81). One sees the contributions of wave propagation therein for $k_z^2+k_y^2<K_D\ k_0^2$ and the contribution of coaxial modes for $k_z^2+k_y^2\cong k_0^2$. The value of the total TE radiated power is indicated. For comparison the figure caption also gives the radiated powers P_{VAC} [19] for vacuum (K_D=1) an P_{COAX} for the coaxial modes when a metal wall or a dielectric medium with $|K_D|\rightarrow\infty$ is placed at in x=-a. Fig. 3b shows that the spectrum shape and magnitude is similar for the plasma case.
For the same range of $k_z^2+k_y^2$ the loading due to the plasma is slightly lower and there is a small asymmetry between the positive and negative values of k_y due to the anisotropy of the plasma. This anisotropy effect is small at high densities.

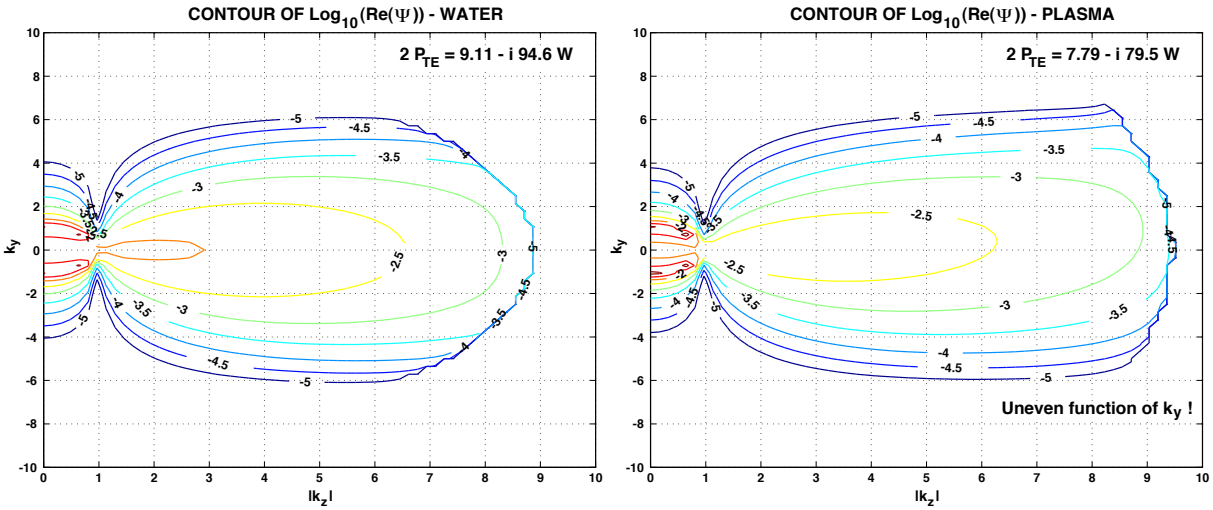

FIG. 3. k_z, k_y spectrum of the real part of the function $\Psi \propto Re\ P_{TE}(k_z,k_y)$. (a) for water loading, (b) for plasma loading (case of a single strap). The corresponding values of P_{TE} are given (values for 1A flowing in the strap). For comparison $Re(2P_{TE})_v$=1.04W for radiation in vacuum (K_D=1) and $Re(2P_{TE})_{coax}$=3.56W for coaxial modes (metal wall at x=-a, a=0.15m).

If losses inside the dielectric are introduced by the addition of an imaginary part K_D" in $K_D=K_D'+iK_D$" or by an equivalent conductivity $K_D"=\sigma/(\omega\ \varepsilon_0)$, a decrease of the antenna loading appears due to the larger reflection at the K_D transition. The shape of the power spectrum is also modified: the propagation of damped waves extends in the domain $k_z^2+k_y^2>k_0^2K_D'$ but this does not compensate the loss of coupling due to higher reflection at the edge x=-a. This is shown in Fig. 4

Description of the SOL by a multi-step dielectric susceptibility profile. Fig. 5 displays the contour of the square of the perpendicular propagation constant of the fast magnetosonic wave $k_\perp^2(|k_z|,n)$ as a function of k_z and of the distance δr from the last closed magnetic surface (LCMS). The plasma density profile in the SOL is given by $n=n_{edge}\exp(-\zeta)$ with $\zeta=\delta r/l_{SOL}$. The LCMS density is $n=n_{edge}$ and l_{SOL} is the density decay length in the SOL. Vacuum conditions for the wave propagation takes place at ~7 scrape-off lengths of the LCMS for the conditions of Fig. 5. To excite waves into the plasma the electromagnetic field corresponding to k_y=0 has to tunnel up to the cut-off for $|k_z|>k0$ and between the cut- off and the resonance for $|k_z|<k_0$. The tunneling distance is larger if $k_y\neq0$. The plasma resonance appearing at low density only leads to weak absorption in the SOL [18].
The effect on the distributed plasma loading resistance R_A (case of single strap) of the decay length l_{SOL} with a constant distance between the antenna and the LCMS is shown in Fig. 6 for

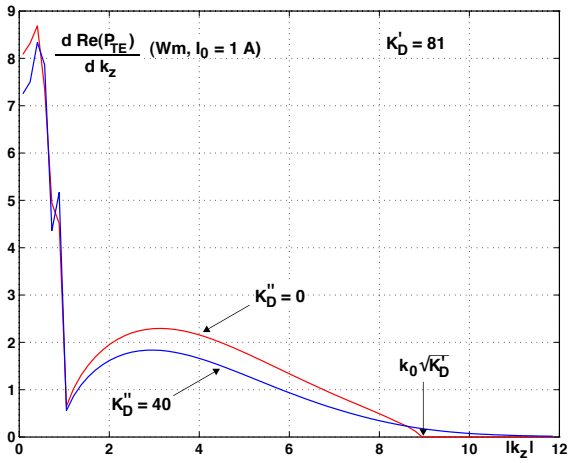

FIG. 4. Effect of losses in the dielectric: k_z spectrum of $Re(2P_{TE})$ for K_D"=40 and K_D"=0.

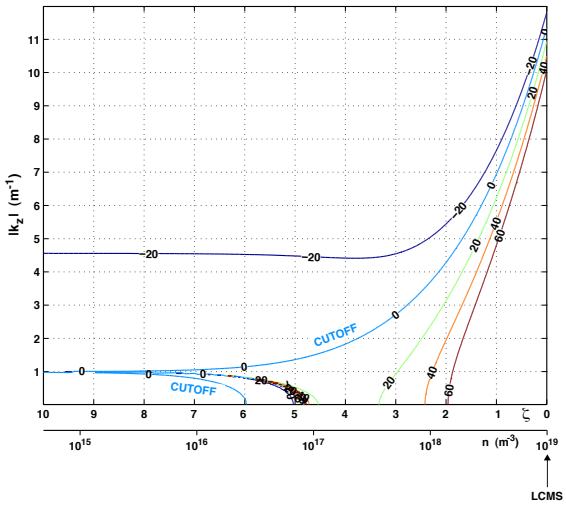

FIG. 5. Contour of $k_\perp^2(/k_z/, n)$ in the SOL for $n=n_{edge}\exp(-\zeta)$ with $n_{edge}=10^{19}m^{-3}$ as a function of $/k_z/$ and ζ (or n). $\zeta=\delta r/l_{SOL}$ where δr is the distance towards the wall starting from the LCMS and l_{SOL} is the density decay length.

ITER relevant conditions. The results neglecting coaxial modes are first given. They correspond to the direct coupling to the plasma through the waves tunnelling between the strap and the cut-off for $|k_z|>k_0$. The effect of increasing l_{SOL} is to decrease this tunnelling distance for a part of the wave spectrum. This loading is well described by a single-step profile of plasma density if l_{SOL} is sufficiently small with respect to the distance LCMS-antenna. The excitation of coaxial modes and surface wave give an additional contribution to the loading which can become equal to or even larger than the one due to the direct coupling if the tunnelling distance becomes large for a large part of the wave spectrum. The magnitude of the coaxial mode contribution depends on the distance "*a*" and on the density profile (see the

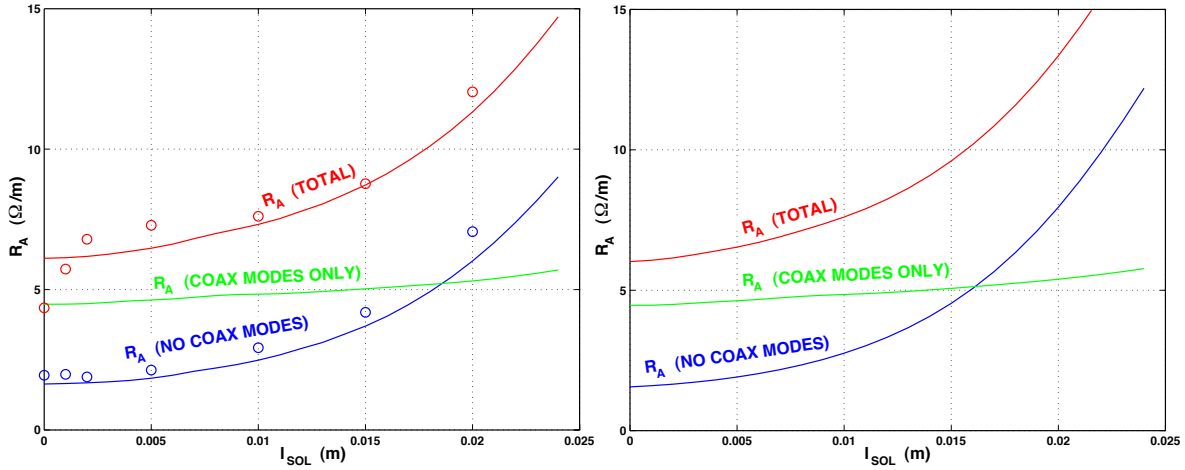

FIG. 6. a) Influence of the SOL decay length l_{SOL} on the loading due to plasma for $n_{edge}=10^{20}m^{-3}$ and distance LCMS-strap=0.15m. The loading due to direct coupling, to coaxial modes and to their sum is shown. Plain lines: Fourier integral evaluation of equation (1), multi-step density profile analysis. Open circles: BRACC results (integration through the exponential density profile and series calculation with R=6.2m and r=2.95m). b) Similar analysis for a dielectric, with multi-step profile of the susceptibility $\chi=K_D-1$. In the plasma bulk we take $K_D=4000+i500$ and in the SOL χ_D proportional to the plasma density step function of a).

discussion in [18]). If a Fourier series is used instead of a Fourier integral to compute R_A, its amplitude exhibits resonances versus the frequency which critically depend on the k_z and k_y steps of the Fourier series [16, 17]. The spectrum density becomes large for the large spatial periods of ITER. As these modes are coupled to each other by the toroidicity and are damped by their coupling to the plasma bulk the Fourier integral probably gives a more realistic estimate of coupling. On Fig. 6a are shown the contribution of the coaxial modes and the total loading resistance obtained from Fourier integral or Fourier series.

The effect of the plasma profile in the SOL can also be taken into account by a multi-step plasma density profile which approximately follows the inhomogeneous plasma profile. On Fig. 6a the continuous curves are obtained from a multi-step density profile with 4 steps per l_{SOL}, and 20 steps in total. At each step the density is decreased by a factor $e^{-1/4}$ and after the last step (of density 6.74 $10^{17}m^{-3}$) the density is set to zero up to the strap. The circles are obtained from numerical integration through the inhomogeneous profile up to 3cm of the strap by the BRACC code. The total loading resistance is obtained from Fourier series by the BRACC code and by Fourier integral for the multi-step density profile: this explains the difference between both results which is larger at low values of l_{SOL} . The loading due to inhomogeneous density profile can fairly be simulated by an inhomogeneous dielectric with a step function in the susceptibility $\chi_d=K_D-1$. Fig. 6b shows the results obtained with a step function in χ_d taken proportional to the density step function of Fig. 6a, such that the last step of the 20 describing the χ_d profile is characterised by $K_D=26.95+i3.37$ before the $K_D=1$ region up to the strap. The similarity between both results is striking. Even a small number of susceptibility steps can give a good description of the effect of the SOL on the coupling.

3. Application to realistic 3D modelling of the JET A2 antenna with MWS

Equivalent dielectric parameters approximating loading conditions to a typical JET ELMy H Mode plasma have been obtained from the above considerations. In a first application we use a single dielectric volume with $K_D=2000$. This value of K_D confirms an earlier ad-hoc choice [6] based on matching the magnetosonic wavelength. A curved dielectric block, shaped like a reference JET divertor discharge and at ≈9.5cm (midplane) from the front face of the straps, is used to load the 3D MWS model of the JET A2 antenna shown on Fig. 7. Power absorption in the plasma bulk is simulated by an outgoing wave condition at five boundaries of the simulation domain, which amounts to assuming effective central single pass absorption. The machine wall is represented by a conducting plane (not shown) at the back of the antenna. This simulation of one half of the array (straps #3 and 4), based on a time-domain analysis and Fourier transform of the results, covers the whole antenna frequency range (23 to 57MHz). Striking features of the results are *(i)* larger high-k// components in the radiation spectrum than assumed in early simulations; *(ii)* a significant fraction of the current flowing on the back side of the straps, i.e. 4.8cm behind the front side. This contributes to explain a lower radiation in the plasma than found with simpler (thin strap, uniform current, box-free) models. Additional details can be found in [6]. Fig. 8 shows the simulated input scattering parameters at the two 30Ω coaxial ports, to be included in a model of the ICRF transmission circuit, and Fig. 9 shows various field outputs. Beside comparison with experimental data, future work will address systematic scans of the antenna-dielectric distance, of the plasma boundary shape, investigation of multilayer dielectric models, modelling the complete 4-strap array and introducing RF losses. Further improvement of the description of plasma loading could be obtained by *(i)* implementing a magnetized plasma in MWS; *(ii)* using the detailed MWS current patterns as sources in the available plasma coupling and heating codes.

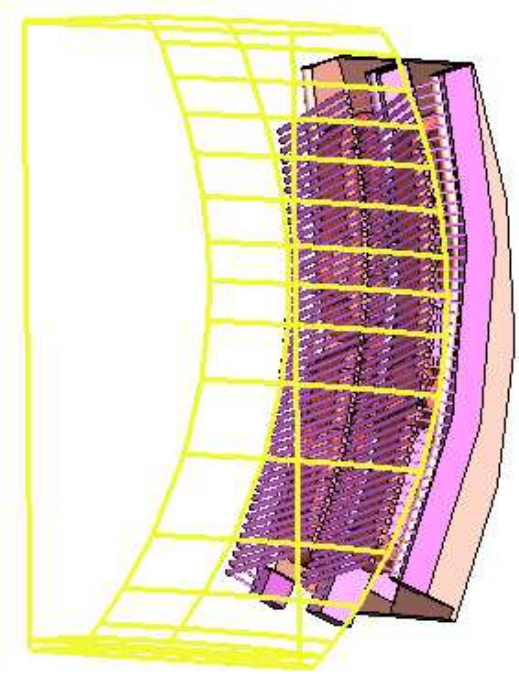

FIG. 7. MWS model of half a JET A2 antenna. Left: strap #4 (‘outer’); right: strap #3 (‘inner’), fed by an in-vessel ‘crossover’ conductor. Coaxial feed lines are at a common toroidal location behind strap 4. The homogeneous dielectric (K_D=2000) is shown as a yellow wireframe.

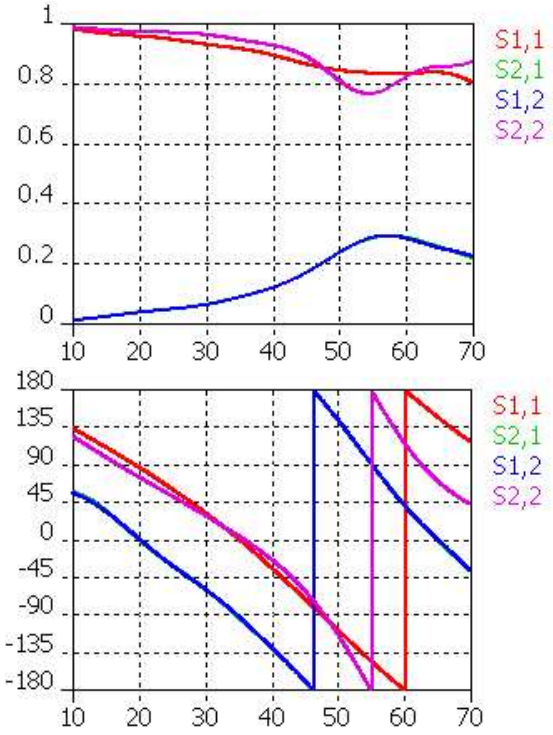

FIG. 8. Computed input scattering parameters vs frequency in MHz. Top: amplitude, bottom: phase in degree. (Port 1 feeds strap 4, port 2 feeds strap 3.) NB S_{21}=S_{12}.

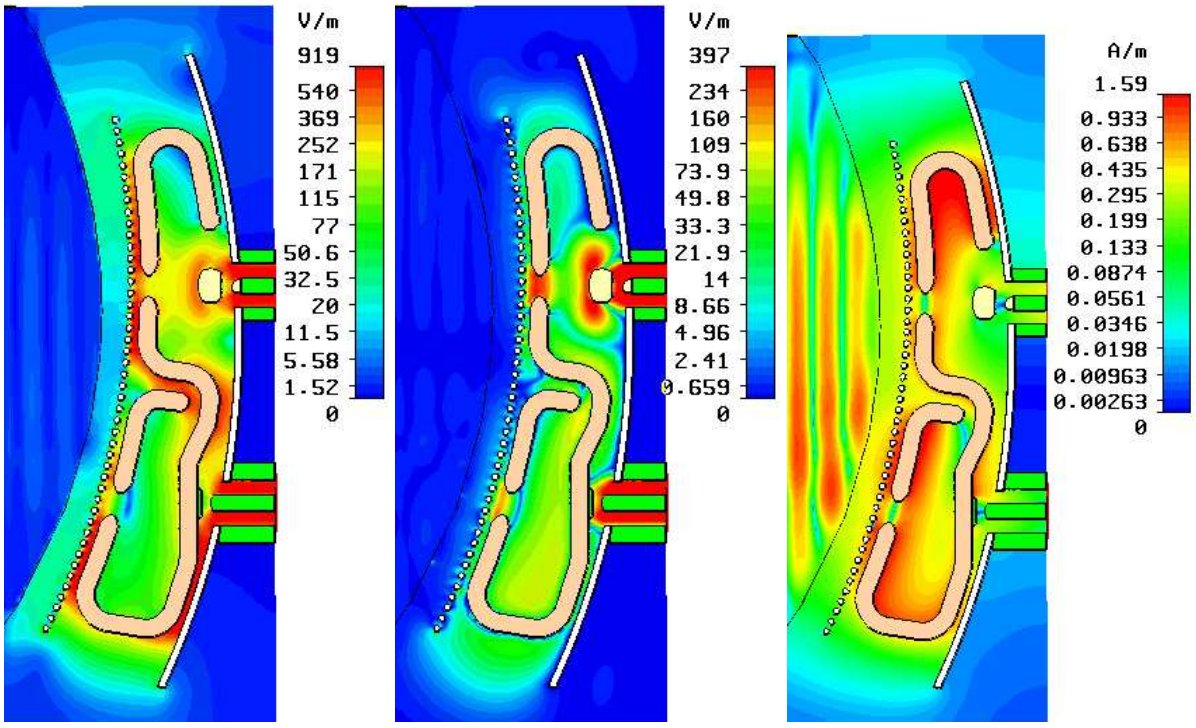

FIG. 9. Vertical cut through strap #4. Left: RF electric field amplitude; centre: toroidal electric field component, mainly confined in the antenna box; right: toroidal RF magnetic field component showing wave propagation in the equivalent dielectric. Toroidal dipole phasing, 42.5MHz. Arbitrary units.

4. Application to testing an ICRH system with a scaled-down mock-up

When decreasing all the lengths of the system and increasing the frequency by the same scale factor f_{MU}, the loading resistance increases by the same factor but the impedance matrix is invariant because the ratio length/wavelength remains constant. There is no need for a large water layer to simulate single pass absorption: addition of salt in the water can easily provide large wave absorption over a short distance [12]. It is also easily possible to vary the loading by changing the distance water tank-antenna "*a*" and therefore to measure the effects of mutual coupling between the straps and e.g. to test the load resilience of an array of straps connected in several "conjugate T" circuits [20]. As an example the mock-up of the ITER antenna with external matching [2] has been constructed with a scale factor f_{MU}=5. All lengths altogether with the distance strap-dielectric are reduced by this factor whereas the frequency is multiplied by it (f=5 × 40-55MHz=200-275MHz) [21].

References

[1] "Technical basis for the ITER Final Design", Sec. 2.5, ITER-EDA Documentation Series 24, IAEA (2001); BOSIA, G., "High-power density Ion Cyclotron Antennas for Next Step Applications", Fusion Science and Technology **43** (2003) 153-160.

[2] MESSIAEN, A. M., *et al.*, in Radio Frequency Power in Plasmas, AIP Conference Proceedings **694** (2003) 142-145; DUMORTIER, P. *et al.*, ibid. 94-97.

[3] DURODIÉ, F., *et al.*, to appear in Proc. 23rd SOFT, Venice, 2004, paper ID 455.

[4] LAMALLE, P. U., *et al.*, ibid. 122-125.

[5] HARTMANN, D., et al., ibid.106-109.

[6] LAMALLE, P.U., et al., Europhysics Conference Abstracts **27A** (2003) P-1.103.

[7] CST GmbH, "CST MICROWAVE STUDIO User Manual", V. 5.0, Darmstadt, Germany, 2003.

[8] ANSOFT Corp., "High Frequency Structure Simulator™", v.8.5, Pittsburgh, PA, USA, 2002.

[9] KAYE, A., *et al.*, Fusion Engineering and Design **24** (1994) 1.

[10] FECHNER, B., "Optimisation des antennes radio-fréquences A2 pour le chauffage cyclotronique ionique sur le tokamak JET", Ph. D. Thesis, Université Aix-Marseille I (1996).

[11] KOCH, R., *et al.*, Computer Phys. Communications **40** (1986) 1.

[12] MESSIAEN, A.M., *et al.*, (2004) Laboratory Report 123, Laboratory for Plasma Physics, Royal Military Academy, Brussels, Belgium.

[13] BRILLOUIN, L., Radioélectricité **3** (1922) 147.

[14] KING, R., "The theory of linear antennas", Harvard University Press (1956).

[15] RAMO, S., et al., "Fields and waves in communication electronics", J.Wiley and Sons (1965).

[16] MESSIAEN, A., et al., Proc. 3rd Joint Varenna-Grenoble Int. Symposium, Vol. 1 p.243.

[17] BHATNAGAR, V., et al., "Plasma Physics and Controlled Nuclear Fusion Research", IAEA, Vienna (1982) Vol.II, p.103.

[18] MESSIAEN, A., et al., Proc. 13th Eur. Conf. Contr. Fusion and Plasma Heating, Schliersee (1986), ECA **10c** II p.125.

[19] STORER, J. and KING, R., Proc. IRE **39** (1951) 1408.

[20] LAMALLE, P. U., et al., to appear in Proc. 23rd SOFT, Venice, 2004, paper ID 218.

[21] MESSIAEN, A., et al., to appear in Proc. 23rd SOFT, Venice, 2004, paper ID 211.